ADVANCED FUNCTIONAL MATERIALS
www.afm-journal.de

Photovoltaic Function and Exciton/Charge Transfer Dynamics in a Highly Efficient Semiconducting Copolymer

Jodi M. Szarko, Brian S. Rolczynski, Sylvia J. Lou, Tao Xu, Joseph Strzalka, Tobin J. Marks, Luping Yu, and Lin X. Chen**

Exciton dissociation is a key step for the light energy conversion to electricity in organic photovoltaic (OPV) devices. Here, excitonic dissociation pathways in the high-performance, low bandgap "in-chain donor–acceptor" polymer PTB7 by transient optical absorption (TA) spectroscopy in solutions, neat films, and bulk heterojunction (BHJ) PTB7:$PC_{71}BM$ (phenyl-C_{71}-butyric acid methyl ester) films are investigated. The dynamics and energetics of the exciton and intra-/intermolecular charge separated states are characterized. A distinct, dynamic, spectral red-shift of the polymer cation is observed in the BHJ films in TA spectra following electron transfer from the polymer to $PC_{71}BM$, which can be attributed to the time evolution of the hole–electron spatial separation after exciton splitting. Effects of film morphology are also investigated and compared to those of conjugated homopolymers. The enhanced charge separation along the PTB7 alternating donor–acceptor backbone is understood by intramolecular charge separation through polarized, delocalized excitons that lower the exciton binding energy. Consequently, ultrafast charge separation and transport along these polymer backbones reduce carrier recombination in these largely amorphous films. This charge separation mechanism explains why higher degrees of PCBM intercalation within BHJ matrices enhances exciton splitting and charge transport, and thus increase OPV performance. This study proposes new guidelines for OPV materials development.

1. Introduction

Photoconducting polymers have been used in organic photovoltaic (OPV) devices as electron donors or p-type materials when blended with electron acceptors such as [6,6]-phenyl-C_{61}-butyric acid methyl ester ($PC_{61}BM$ or PCBM) for over 15 years.[1–9] In particular, poly-3-hexylthiophene (P3HT) set a historical benchmark as the material yielding the highest power conversion efficiency (PCE)[2,10,11] until several years ago, when new series of lower bandgap polymers emerged offering higher PCEs.[9,12–15] Unlike homopolymers such as P3HT, that have a single building block in each repeat unit, these lower bandgap polymers contain alternating building blocks in each repeat unit. Because of the electron affinity difference between the alternating blocks, these new copolymers have in-chain charge transfer characteristics that enhance broad absorption in both the UV/vis and near-IR regions.[16,17] The lower bandgap versus P3HT enables more effective solar photon harvesting, especially in the near-IR region. One of the most promising new

Dr. J. M. Szarko, Dr. B. S. Rolczynski, S. J. Lou, Prof. T. J. Marks, Prof. L. X. Chen
Department of Chemistry
Northwestern University
Evanston, IL 60208, USA
E-mail: lchen@anl.gov
Dr. J. M. Szarko, Dr. B. S. Rolczynski, S. J. Lou, Prof. L. X. Chen
Chemical Sciences and Engineering Division
Argonne National Laboratory
Argonne, IL 60439, USA
Dr. J. M. Szarko, Dr. B. S. Rolczynski, S. J. Lou, T. Xu, Prof. T. J. Marks, Prof. L. Yu, Prof. L. X. Chen
Argonne-Northwestern Solar Energy Research (ANSER) Center
Northwestern University
2145 Sheridan Road, Evanston, IL 60208, USA
E-mail: lupingyu@uchicago.edu
T. Xu, Prof. L. Yu
Department of Chemistry and
The James Franck Institute
The University of Chicago
929 E 57th. Street, Chicago, IL 60637, USA
Dr. J. Strzalka
X-ray Science Division
Advanced Photon Source
Argonne National Laboratory, Argonne, IL 60439, USA

DOI: 10.1002/adfm.201301820

Jodi M. Szarko received her B.A. from Wesleyan University and her Ph.D. from the University of Colorado at Boulder. After working at the Helmholtz Centrum Berlin, she is currently a Postdoctoral Researcher at Northwestern University. Her main focus is on the structural and kinetic properties of organic photovoltaics.

Brian S. Rolczynski earned his Ph.D. in Chemistry from Northwestern University, where he studied the intersection between nanoscale aggregation characteristics and ultrafast dynamics in alternating copolymers for organic, bulk heterojunction solar cells. Previously, he received a B.A. in English and B.S. in Chemistry from the University of Washington. He is currently a postdoctoral researcher at the University of Chicago.

Joseph Strzalka earned his B.S.E. degree at Princeton University and his Ph.D. degree from the University of Pennsylvania. His research in X-ray and neutron scattering from biomaterials has employed user facilities at Brookhaven, Argonne and Los Alamos National Laboratories, as well as the NIST Center for Neutron Research. Since 2008 he has been a staff scientist for Beamline 8-ID-E of the Advanced Photon Source, Argonne National Laboratory.

Tobin Marks received a B.S. from the University of Maryland and a Ph.D. from MIT. He is a member/fellow of the U.S., German, and Indian National Academies of Sciences, the U.S. NAE, the Royal Society of Chemistry, and the American Academy of Arts and Sciences. He is Professor of Chemistry and Materials Science at Northwestern.

Luping Yu was born in Zhejiang Province, People's Republic of China. He received his B.S. (1982) and M.S. (1984) degrees in polymer chemistry from Zhejiang University and his Ph.D. degree (1989) from The University of Southern California. He is currently a Professor of Chemistry at the University of Chicago. His present research focuses on polymer chemistry.

Lin X. Chen is a Senior Scientist in Argonne National Laboratory and a Professor of Chemistry at the Northwestern University. Her current research is focused on transient molecular structural studies in solar energy conversion processes and structures-dynamics-efficiency correlations in organic photovoltaic materials. She received her B.Sc. from Peking University, Ph.D. from the University of Chicago, and did postdoctoral research in the University of California at Berkeley. She is an AAAS Fellow.

polymers is a fluorinated poly-thienothiophene-benzodithiophene, PTB7, which has regularly alternating thienothiophene (TT) and benzodithiophene (BDT) blocks in each repeating unit (**Figure 1**). OPVs fabricated with from this polymer and PCBM achieve >8% PCEs.[18,19]

In addition to the enhanced light harvesting/increased PCEs, PTB7 exhibits unique exciton dynamics, and structural morphologies have been observed in solution and films.[20–23] Because of the differences in electron affinities between the TT and BDT blocks, the local electron density exhibits "push–pull" tendency along the conjugated polymer backbone; one block (BDT) acts as a quasi-electron donor (or pusher) and the other (TT) as a quasi-electron acceptor (or puller) (Figure 1). The role of the charge transfer (CT) states at the polymer:PCBM domain interfaces in low bandgap polymer BHJ films has been studied in several systems.[16,24] In contrast, the role of CT states and their dependence on the push–pull character within each of these polymers has received little attention in the context of OPV science since these intramolecular charge transfer/separation processes were thought to be unimportant for device performance. Before further discussions, we should first define the CT state because its definition varies slightly among the researchers in the field. The CT state in this report is defined as the state resulted from the exciton splitting with a lower

Adv. Funct. Mater. **2013**,
DOI: 10.1002/adfm.201301820

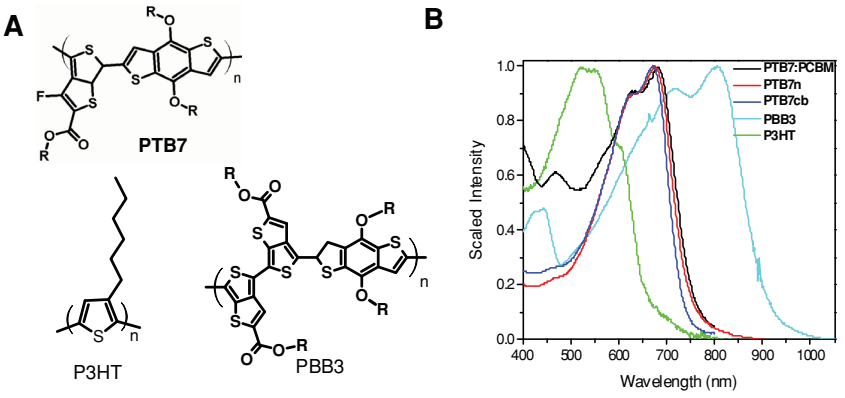

Figure 1. A) Structures of PTB7, P3HT, and PBB3. B) Optical spectra of PTB7(cb), PTB7(n), and PTB7:PCBM.

energy while hole and electron are still strongly interacting, and displays a distinct transient absorption spectral feature blue-shifted from that of the polymer cation. In comparison, the charge separate (CS) state is defined as a state resulted from the exciton splitting with weaker hole–electron interactions than those in the CT state, and displays a polymer cation absorption signature (hence, this state is also called polymer cationic state below).

Several unique properties of the PTBX polymers were observed in previous studies.[20,21,25–27] First, structural studies of seven neat PTBX polymers with different pendant alkyl substituents showed that the copolymer film crystallinity was relatively low and that the films were largely amorphous.[20,22] Second, the as-prepared PTBX:PCBM BHJ films showed well-mixed donor and acceptor components with apparent domain sizes <5 nm, and higher PCEs than those films having more ordered morphologies after annealing at higher temperatures (i.e., 160 °C).[26] Third, a substantial cation state population due to intramolecular exciton splitting was observed in PTB7 even in dilute solutions, generating a pseudo-charge transfer and cationic states in the absence of the PCBM electron acceptor.[21] Although charge transfer states of other polymers in BHJ and neat films have been investigated, they have not been clearly identified in isolated solution phase polymer chains, and intramolecular exciton splitting has been assumed to be negligible in the isolated conducting polymer chains.[28–42]

Therefore, there are important unanswered scientific questions regarding the structure/dynamics dependence of BHJ PCEs, particularly those fabricated with PTB7. How does the electronic structure of the copolymer backbone facilitate charge generation and transport? Do the intramolecular (or intrachain), charge-separated states affect intermolecular (or interchain) interactions in a BHJ film? How do the smaller crystalline domains affect carrier transport in the PTB7 films? What is the mechanism for overcoming the Coulombic attractions between the separated electrons and holes in the BHJ films after the initial exciton splitting?

In this contribution, we focus on the effects of both intrachain and interchain PTB7 charge transfer characteristics and how these affect exciton-splitting efficiencies and dynamics in OPV BHJ films. In particular, the ultrafast dynamics of the exciton splitting and marked presence of the PTB7 cation population in the absence of an external electron acceptor, such as PCBM, prompts us to investigate the exciton splitting mechanisms in various media which differ from those of homopolymers such as P3HT. The stark differences in both exciton splitting dynamics and structural/morphological characteristics of PTB7 films (neat and BHJ) from those of P3HT make it necessary to reassess the optimal film morphologies for OPV devices fabricated from these new materials. Mechanisms of charge separation and carrier diffusion in PTB7 in solution, neat films, and BHJ films are discussed on the timescales of sub-picoseconds to nanoseconds. Because PTB7 shares many common features with other recently synthesized "in-chain donor–acceptor" polymers that afford high PCEs, we suggest PTB7 as a model to demonstrate the need to reevaluate the necessary conditions and mechanisms for exciton splitting and charge carrier generation in in-chain donor–acceptor copolymers. Such a re-evaluation is discussed in the context of other polymers that have recently been studied by the OPV community.

2. Optical and Electronic Characteristics of PTB7

2.1. Sample Preparation and Analysis

PTB7 was synthesized according to a previously reported procedure.[43] For the solution studies, the polymer was dissolved in chlorobenzene (CB), and had an optical density between 0.2 and 0.4 at the wavelengths of the excitation using 2-mm cuvettes. Steady-state absorption spectra were taken using a Shimadzu UV-3600 spectrometer. The preparation conditions for the spin-cast films was reported previously.[20] Briefly, the films were prepared from a (10 mg mL^{-1}) 1,2 dichlorobenzene (DCB) solution and spin-cast at speeds from 3000–5000 rpm. For the PTB7:PCBM blend films, the solution also contained 3 vol% of the processing additive 1,8-diiodooctane (DIO) which increases the device PCE.[44] The films were then spin-cast onto ITO or glass substrates. This report focuses on three types of samples: PTB7 in CB, neat PTB7 films, and PTB7:PCBM BHJ films. These samples will be denoted PTB7(cb), PTB7(n), and PTB7:PCBM, respectively.

2.2. Steady State Absorption Spectra of PTB7

The steady state absorption spectra of PTB7(cb), PTB7(n), and PTB7:PCBM are shown in Figure 1. The principle absorption maximum of the solution spectrum is at 682 nm, adjacent to a feature at 633 nm, and separated energetically by ≈1125 cm^{-1}, which coincides with the thiophene ring stretching frequency.[45] Hence, the two peaks are vibronic bands. The extinction coefficient of PTB7(cb) in terms of monomer units is approximately 10 000 M^{-1} cm^{-1} at 690 nm. These PTB7 vibronic peaks are also observed in the films, with the neat film absorption maximum at 687 nm only slightly red-shifted from that in solution. Such a

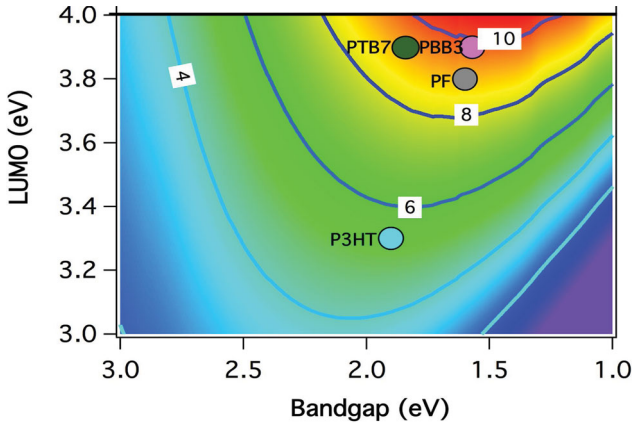

Figure 2. A contour plot showing the calculated power conversion efficiency (values marked on the contour lines) as a function of the polymer band gap and the LUMO.

small red-shift indicates very slightly increased planarity in the films, while the vibronic energy spacing remains unchanged. Finally, the addition of PCBM to the films results in a further small red-shift of the absorption maximum to 690 nm while the vibronic energy spacing increases to 1300 cm^{-1}. The spectra of blend films deviate from those reconstructed by a principle component analysis procedure using the spectra of the neat PTB7 and $PC_{71}BM$ films. Therefore, the intermolecular interactions of these two species are sufficiently strong in BHJ films to alter their electronic and vibrational properties. It has been found that the PCBM is well intercalated into the PTBX polymer,[20,22] which can create charge transfer states and induce absorption spectral red-shifts.

2.3. Bandgap Alignment of PTB7 and its Effect on Solar Cell Efficiency

Originally, the impetus for using donor–acceptor copolymer OPV materials was to increase the spectral overlap with the solar spectrum. Although the enhancement of the light harvesting was accomplished in these copolymers, the PCEs of these materials still vary widely.[25] Comparison of the bandgap alignment of several polymer systems, along with their maximum possible efficiencies, is shown in **Figure 2**. The solar cell parameters of the devices depicted in ths figure are shown in **Table 1**. The maximum efficiencies shown are calculated from the model of Scharber et al.,[46] where the balance of exciton splitting driving force, band gap, solar energy spectrum, and output voltage are taken into account. The bandgap of P3HT is over 1.9 eV, which is the largest and has the lowest spectral overlap.[16] The maximum estimated efficiency for solar photon harvesting using this bandgap is 42%. In contrast, the bandgap of PTB7 is ≈1.6 eV, which corresponds to a maximum solar photon harvesting efficiency of 58%.[16,47–49] The theoretical OPV PCE maximum with respect to both the donor band gap and the donor lowest unoccupied molecular orbital (LUMO) energy levels shows that the optimal bandgap for device efficiency is 1.5–1.6 eV, which is very close to the PTB7 bandgap. The highest theoretical PCE based on the bandgap and the relative band level alignment of the donor and acceptor materials is roughly 8–10%, which is close to the PCEs of >8% for current PTB7:PCBM devices.[50] We are aware of some ongoing theoretical work reassessing the band alignment with consideration of molecular details at the interface, while the model discussed here is an approximation without the structural details. From the polymers listed here, it is apparent that there is a large range of PCE values compared to the theoretical maxima for each polymer. While structural and dynamics studies have been performed on these materials, there has not yet been a model to account for these discrepancies. In the sections of this contribution which follow, we propose elements of a picture explaining why the efficiencies of these polymer systems vary so greatly.

Table 1. The solar cell parameters of select donor-acceptor polymers.

	E_g	V_{oc} [V]	J_{sc} [A cm^{-2}]	FF	η
PF[51]	1.6	0.59	10.22	0.40	2.38
P3HT[5]	1.9	0.63	9.5	0.68	5.0
PTB7[52]	1.84	0.74	14.3	0.69	>8
PBB3[52]	1.57	0.63	6.37	0.51	2.04

Recently, new copolymer and oligomer systems have enabled OPV PCEs exceeding 9%;[53] however, the structures of these materials have not been made public. Indeed many copolymers exhibit similar or more optimal bandgap alignment than these high-performance polymers, however their corresponding PCEs can vary significantly. Such variations prompt us to look beyond the bandgap energy alignment and to scrutinize local intramolecular interactions and features of the polymer electronic structure. In recent studies, we reported strong correlations between calculated changes in the repeat unit ground to the excited state dipole moment of these polymers and their corresponding OPV PCEs.[52,54] For two of the polymers examined here, PTB7 and PBB3, the ground and excited state dipole moments, μ_g and μ_e in their respective single repeat units are characterized as in **Figure 3**. Although PBB3 has a more optimal bandgap alignment, its dipole moment change is small, and the OPV PCE is significantly less than that of PTB7 with a much larger $\Delta\mu_{ge}$. The larger PTB7 $\Delta\mu_{ge}$ enhances the charge transfer character, and therefore the carrier generation efficiency in the corresponding BHJ films, as discussed below.

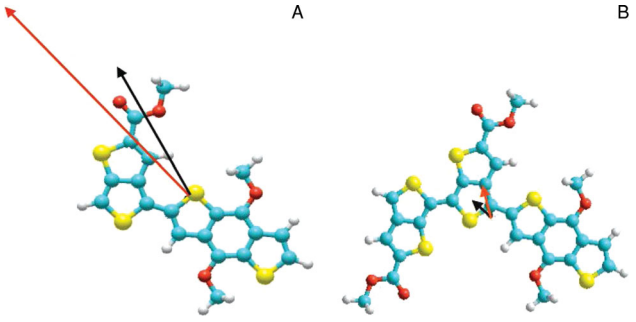

Figure 3. The backbone structure of the PTB7 and PBB3 polymers. The ground state dipole moments are indicated by the black arrows while the excited state dipole moments are indicated by the red arrows. Adapted from previous work.[52]

Adv. Funct. Mater. **2013**,
DOI: 10.1002/adfm.201301820

3. PTB7 Exciton and Charge Transfer Dynamics in Different Environments

3.1. Transient Absorption Spectroscopy

The steady state absorption spectra of the PTB7 (cb), PTB7(n), and PTB7:PCBM were recorded using a Varian Cary 50 Scan (Agilent Technologies, Santa Clara, CA) before and after transient absorption (TA) experiments to verify the sample stability during the TA experiments. The TA experiments were performed at the Center for Nanoscale Materials or the Chemical Sciences Division at Argonne National Laboratory. A visible pump beam at 1.67 kHz or 1 kHz was generated by either an optical parametric amplifier (OPA) system (TOPAS, Light Conversion Ltd.) or a home-built two-pass OPA system and pumped by a regenerative amplifier (Spitfire Pro, Spectra Physics Lasers) operating at a 5 kHz or 1 kHz repetition rate. The Spitfire Pro was pumped by an Nd:YLF laser (Empower, Spectra-Physics Lasers), and seeded by a Ti:sapphire oscillator (Tsunami, Spectra-Physics Lasers) that was pumped by a Nd:YVO_4 laser (Millennia, Spectra Physics Lasers). The output beam of the amplifier laser was split off and chopped at 833 Hz. These beams were used to pump a TA spectrometer (HELIOS, Ultrafast Systems LLC). A white light/NIR probe was generated by focusing the 800 nm beam into a sapphire plate. The 800–1500 nm component of this probe light was collected by a charge-coupled device CCD device. The spectral detection region is 850–1500 nm. The solution sample was prepared and probed in ambient air while stirring. The samples were robust in this environment and exhibited unchanged kinetics over the course of the measurements. The films were raster scanned or moved under ambient conditions.[55] Samples were pumped using a focused 100 µm diameter, 20 nJ per pulse. The pump wavelength was 600 nm unless stated otherwise. The cuvette path length was 2 mm, and the instrument response function (IRF) was 160 fs FWHM. For film experiments, the transmission of prepared films on glass substrates was measured, and the response function was 120 fs.

3.2. PTB7 Exciton and Charge Transfer Kinetics in Different Environments

TA spectra in the near IR region for PTB7 (cb), PTB7(n), and PTB7:PCBM are shown in **Figure 4** as a function of probe delay time specified by the color scale bars, and with >300 delayed TA spectra in each set of data. Using a detailed deconvolution

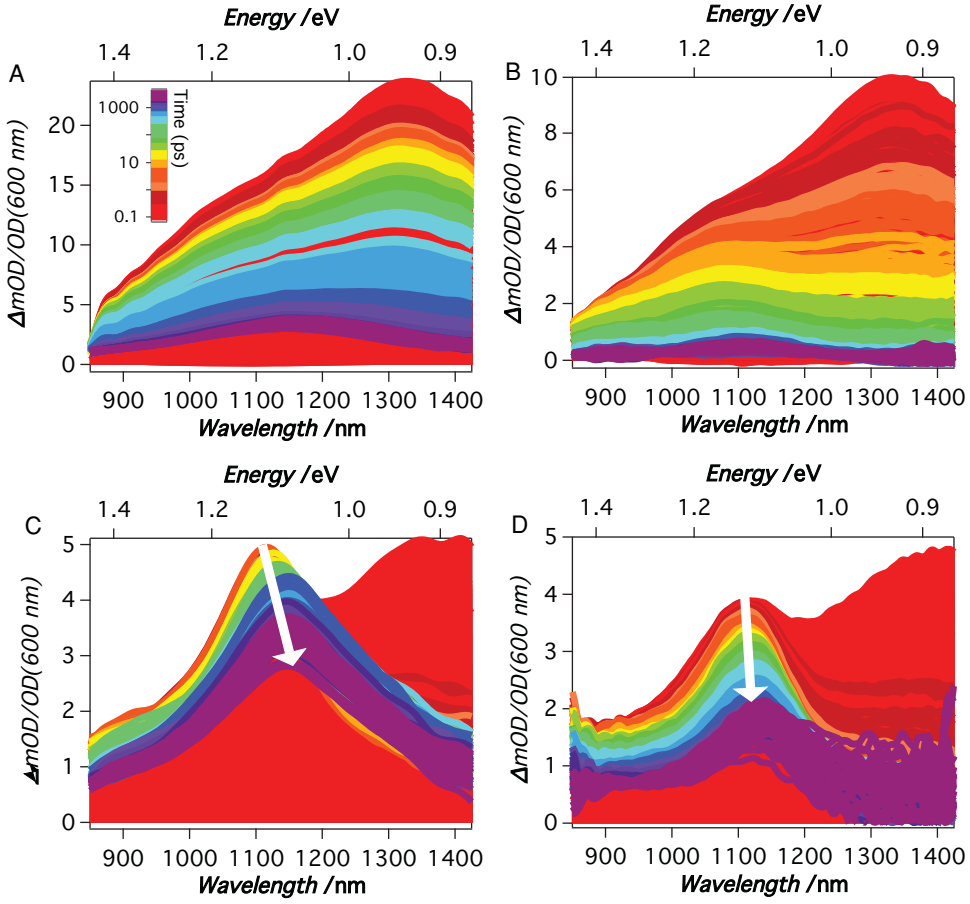

Figure 4. Transient absorption spectra of PTB7 in different media: A) 1,2-dichlorobenzene, B) a neat film, and C) PTB7:PCBM. The probe delay times of the spectra are color coded from red to purple shown in the color scale bar on the left. The excitation wavelength is 600 nm. D) The transient absorption spectra of the PTB7:PCBM film under the 695 nm light excitation.

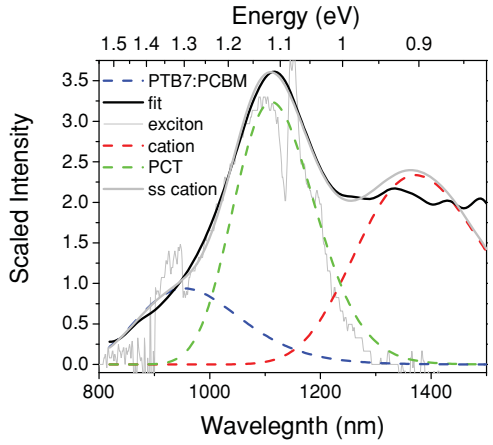

Figure 5. The graphical representation of the exciton (red), cationic (green), and pseudo charge transfer states (blue) used to fit the kinetics of these states. The steady state chemically oxidized cationic state is also shown in gray.

procedure, three broad peaks in each individual TA spectrum were extracted and analyzed, corresponding to the exciton state (EX), cation state (CS), and (pseudo) charge transfer state (PCT, intramolecular, or CT, intermolecular).[21] The individual contributions from these states to the overall transient absorption spectra of PTB7:PCBM are extracted and shown in **Figure 5**. The kinetics of these three states were extracted from the TA spectra using Equation 1, where $A(t,\omega)$ is the total TA signal at time delay time t and probe frequency ω; PCT(ω), CS (ω), and

$$A(t,\omega) = a_1(t)\,\mathrm{PCT}(\omega) + a_2(t)\,\mathrm{CS}(\omega) + a_3(t)\,\mathrm{EX}(\omega) \quad (1)$$

EX(ω) are the fit spectra of PCT (or CT), CS, and EX, respectively (Figure 4). $a_1(t)$, $a_2(t)$ and $a_3(t)$ are the amplitudes of PCT (or CT), CS, and EX, respectively, at t. The EX and CS are the main focus of this study.

The kinetics of EX in PTB7(cb), PTB7(n), and PTB7:PCBM are shown in **Figure 6**a with fitting parameters summarized in **Table 2**. The faster overall decay kinetics in the neat film compared to the solution are attributed to additional EX decay channels through interchain charge transfer or geminate recombination mechanisms.[56] In solution, the CS state is mainly generated via an intramolecular process as shown by the concentration independent TA kinetics in our TA measurements. In comparison, the intermolecular interactions in the films are much stronger due to the π–π backbone stacking.[57–58] The TA spectra of the BHJ films (Figure 4c) are markedly different from those of PTB7(n) (Figure 4b). The EX state, with its TA feature peaked near 1320 nm, is almost completely depleted within 1 ps of the excitation, and simultaneously the signal from the CS state peaked near 1150 nm rises, indicating that the CS state becomes the predominant species within a few ps of excitation and persists on a timescale much longer than the 3-ns time window of these measurements. The CS state dynamics in the presence of PCBM in the BHJ film indicate highly efficient and ultrafast charge transfer from PTB7 to PCBM.

The CS kinetics traces in solution and in the films are shown in Figure 6b, with the corresponding tri-exponential fitting parameters summarized in Table 2. The amplitudes

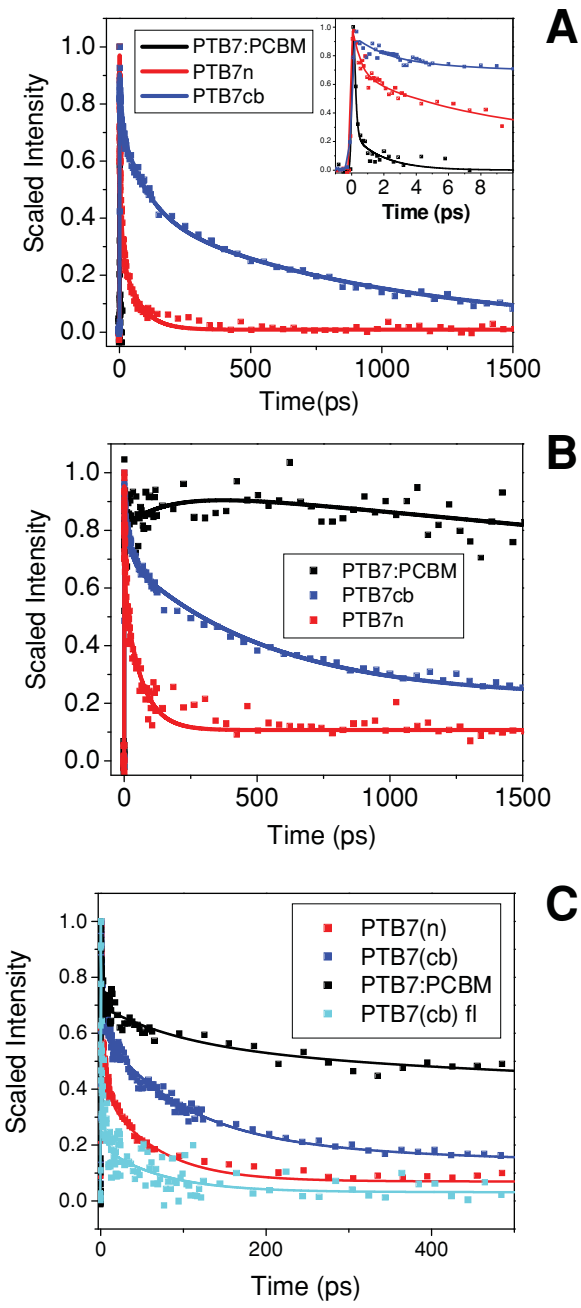

Figure 6. The experimental data (solid squares) and kinetics fits (solid curves) of A) the EX state, B) the CS state, and C) the ground state bleach for PTB7(cb) (red), a PTB7(n) (blue), and PTB7:PCBM film (black). The fluorescence upconversion signal for PTB7(cb) is also shown in light blue.

of the component with the longest time constant are proportional to the population of the sustained CS state that survives the fast h^+–e^- recombination or charge recombination (CR). A much smaller amplitude of CS signals in PTB7(n) than in PTB7(cb) suggests that CR is much faster in the former due to the additional relaxation channels through intermolecular processes. In contrast, CS kinetics in the PTB7:PCBM film feature an ultrafast rise within the instrument response time (<150 fs) followed by the second slower rise with 116 ps rise

Adv. Funct. Mater. **2013**,
DOI: 10.1002/adfm.201301820

Table 2. Kinetic fits for the exciton, charge transfer, and cationic states of PTB7(cb), PTB7(n), and PTB7:PCBM. The relative amplitude of each fit is given as a percentage and is indicated in the parentheses.

Sample	Exciton decays [%A]	CT decays [%A]	Cation decays [%A]
PTB7(cb)	2.5 ps (21%)	2.5 ps (21%)	20 ps (22%)
	100 ps (33%)	500 ps (61%)	550 ps (53%)
	900 ps (46%)	>>3 ns (18%)	>>3 ns (25%)
PTB7(n)	0.46 ps (37%)	1 ps (–4%)	8 ps (55%)
	7 ps (35%)	120 ps (85%)	130 ps (37%)
	65 ps (28%)	>>3 ns (11%)	>>3 ns (8%)
PTB7:PCBM	<<120 fs (89%)	116 ps (34%)	116 ps (–13%)
	1.7 ps (11%)	>>3 ns (66%)	>>3 ns (87%)

(34%) and a >>3 ns decay (66%). Finally, the ground state bleach (GSB) kinetics are shown in Figure 6c. A red-shift in the GSB spectrum was observed, which indicates the presence of stimulated emission and vibrational relaxation, and charge transfer, which is overlapped with this signal.[33,59] The presence of absorption states heavily masks the emission signals in the TA spectra so the fluorescence lifetime was obtained using a fluorescence upconversion setup for the PTB7(cb) sample. This signal shows a predominate sub-picosecond decay for the fluorescence, which indicates some charge transfer character of the excited state. The GSB kinetics shows a multiexponential decay. The PTB7(cb) and PTB7(n) samples have the same kinetic signatures as the exciton kinetics. The sub-picosecond decay is attributed to exciton annihilation vibrational relaxation, and pseudo charge transfer, which also correlates with the upconversion signal. A decay >>3 ns is also observed. This signal is attributed to long lived charge transfer or triplet states, and is less than ten percent of the overall signal amplitude in the PTB7(cb) and PTB7 (n) signals. The PTB7:PCBM sample has the largest amplitude of this state, which corresponds to the higher degree of free charge carrier generation in the BHJ films.

Because the CS state is the precursor of the free charge carriers in OPV devices, optimizing the relative CS populations is essential for enhancing device performance. The TA spectra at the delay time $t = 2$ ns for all of the present samples are dominated by CS state signals (**Figure 7**a) and hence, they can be used to measure the efficiency of initial CS state generation when normalized by the initial exciton signals. Note that TA signals from the films are noisier than those from the solution due to imperfect film optical quality which causes TA signal scattering. Thus, the relative change in transient optical densities with respect to that of the initial EX signals was measured, which in turn was obtained from the amplitude of the EX fits, between the neat films and the solution, so that the scattering effects could be taken into account. This approximation is the best direct experimental comparison for the relative amplitudes of the long-lived CS states among the samples under the present experimental conditions. After this correction, it is found that the PTB7:PCBM films show the highest CS state signal amplitudes, while PTB7(n) has the lowest, which can easily be explained by increased CR pathways in the films in the

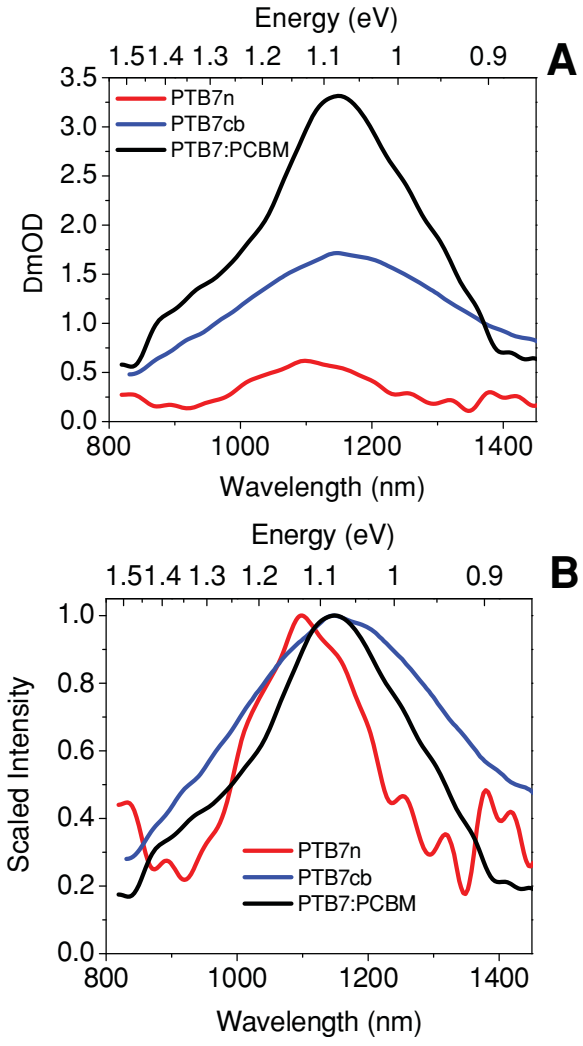

Figure 7. The transient absorption spectra of PTB7(cb) (red), PTB7(n) (blue), and PTB7:PCBM film (black) taken 2 ns after 600 nm excitation from an ultrafast laser pulse. The absorbance for each signal was scaled according to the optical density (OD) in the UV/vis spectra at 600 nm for all samples. The light scattering effects in the samples were corrected by the ΔOD ratio of the EX state at delay time = 0 ps in the neat film and solution.

absence of the PCBM external electron acceptor. It is perhaps unexpected that the CS population in solution is ≈1/2 of that in the BHJ films, suggesting the importance of intramolecular processes in free charge carrier generation, hence device performance.

To compare the TA spectral shapes of the CS state in the three media, the three spectra in Figure 7a were normalized to the peak intensity, and are shown in Figure 7b. In addition to the variation of CS populations among the three samples, the CS peak positions in the TA spectra were also examined. The CS state peak position of PTB7(n) is significantly blue-shifted and has the lowest amplitude relative to that in the solution and in the BHJ films. An apparent correlation between the peak position and the amplitude of the CS state TA signals is

observed in these samples: a larger red-shifted peak position is accompanied by a higher CS state population. It is assumed that the CS state TA features originate in transitions from the cation state to its higher energy excited states that have energies nearly independent of the environment, and hence are nearly isoenergetic across the samples. Thus, the red-shifted CS state peak corresponds to a smaller energy gap between the CS state and its higher energy excited states, and therefore to a higher energy for the CS state in solution and in BHJ films. In comparison, a bluer CS TA peak in PTB7(n) corresponds to a larger energy gap to the higher energy excited state, and hence a lower energy for the CS state. According to the Onsager theory[28] that describes the electrostatic interactions between holes (h) and electrons (e) in continuous media at thermal equilibrium, the energy differences in the CS state energies are primarily due to the Coulombic attraction between electrons in the PCBM domains and holes in polymer domains, which scales inversely with the h–e distance $R_{h\text{-}e}$ that is small at the donor–acceptor interface, resulting in a lower CS state energy versus that summed for holes and electrons as free carriers. Although the Onsager theory is based on a thermally equilibrated system in terms of calculating the capturing radius for a h–e pair, the part of the theory describing the nature of the electrostatic interactions is still applicable to the systems studied here on the ultrafast time scale. Because of the intramolecular CS in PTB7, the average h–e distance after the EX splitting is greater[21] and the Coulombic attractions within in the h–e pair are smaller at the PTB7:PCBM interface than in homopolymers where the intramolecular CS is far less. More interestingly, a continuous CS state peak shift is observed in the TA spectra as a function of the delay time in the PTB7:PCBM films, corresponding to a continuous rise in the CS state energy. A detailed analysis is presented below.

3.3. Dynamics and Spectral Characteristics of Carrier Dissociation in PTB7:PCBM Films

The TA feature in the PTB7:PCBM BHJ films beyond the first few ps delay time is overwhelmingly from the cationic state of PBT7 (Figure 4c). Because the CS state is considered to be a precursor of free charge carriers, its dynamics in BHJ films can be directly related to device PCEs. The CS state dynamics traces of the three samples are shown in Figure 6b. The CS state signals in the PTB7:PCBM BHJ film appear instantaneously followed by a 116-ps rise and then decay with a time constant >> 3 ns. The ultrafast formation of the CS state has been confirmed by both the EX decay and the intramolecular CS state formation in PTB7(cb) and PTB7(n). The second rise component of the CS state with the 116-ps time constant in the BHJ films indicates an additional route for the CS state formation from a bound h–e pair intermediate state that further dissociates on this time scale. This rise-time constant also corresponds to the time constant for a red-shift of the CS state peak position, which is discussed further below.

To characterize the marked dynamic red-shift of the BHJ film CS state peak, a global analysis was carried out on the TA data sets with the TA spectral features versus the probe delay time, allowing the peak position and width of the CS signals

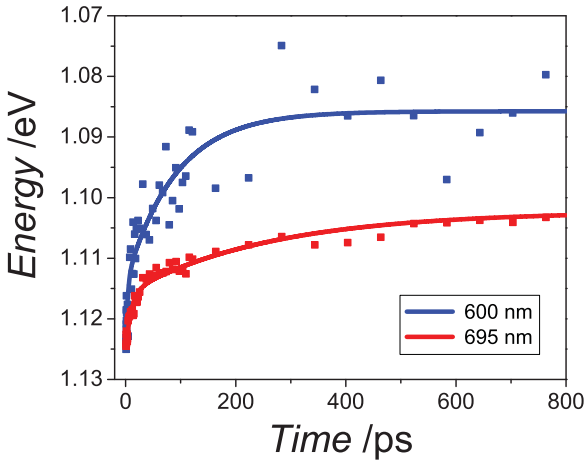

Figure 8. The peak position energy for the CS state using 600 nm (blue) and 695 nm (red) light excitations. The time constants for the red-shift of the peak position extracted from these curves are 90 ps and 261 ps with the excitation wavelength at 600 nm and 695 nm, respectively.

to vary. This analysis showed that a single CS spectral shift with the delay time provides the best fit of the experimental data. By allowing the peak position to vary, the shift of the CS energy level as a function of time can be monitored as shown in **Figure 8**. Two time constants of 3 ps and 90 ps are obtained for the dynamics of the spectral shift. The 3-ps component is attributed to vibrational relaxation of hot CT/CS state in the films,[60] while the 90-ps component is attributed to the thermally activated carrier dissociation.[61] There has been lively discussion recently concerning the nature of the excitation wavelength dependence in charge transfer states.[62–65] Most reports discuss the kinetics of the delocalization of CT states on a timescale less than 200 fs. Note that the results presented in this work regarding the red-shift of the CS state have a faster component which is in the ps range, however the longer decay component cannot be explained using a hot exciton model alone. The longer excitation wavelength dependence in the PTB7:PCBM films indicates the presence of longer lived delocalized CT and CS states that can be populated more readily at higher energies. The long lifetime component is attributed to the dissociation rate of the CS state from the donor/acceptor interface. This dissociation rate is very fast for the present BHJ films compared to previous studies[61,66] and will be discussed in detail below. The initial instantaneous h–e dissociation from the polarized exciton in this donor–acceptor or charge transfer polymer elevates the CS energy levels, which in turn reduces the energy gap between CS and higher energy states, and red-shifts the CS state TA spectrum.[67] Within this time frame, the peak position for CS state TA spectra in the PTB7:PCBM film is red-shifted and becomes broader. The amplitudes of these shifts are summarized in **Table 3**, and indicate an increase of the cation state energetic inhomogeneity in the film.

To further characterize the nature of the time dependent TA cation peak red-shift for the CS state in PTB7:PCBM, the excitation wavelength dependent EX and CS state dynamics of the PTB7(n) and PTB7:PCBM materials were investigated.

Adv. Funct. Mater. **2013**,
DOI: 10.1002/adfm.201301820

Table 3. Wavelength excitation dependence of the lifetimes spectral shift of the cationic state in PTB7:PCBM.

Sample	Exciton decays [%A]	CT decays [%A]	Cation decays [%A]
600 nm			
neat PTB7	0.46 ps (37%)	1 ps (–4%)	8 ps (55%)
	7 ps (35%)	120 ps (85%)	130 ps (37%)
	65 ps (28%)	>>3 ns (11%)	>>3 ns (8%)
PTB7:PCBM	<<160 fs (89%)	116 ps (34%)	116 ps (–13%)
	1.7 ps (11%)	>>3 ns (66%)	>>3 ns (87%)
695 nm			
neat PTB7	0.2 ps (46%)	22 ps (50%)	2 ps (56%)
	5 ps (29%)	224 ps (47%)	59 ps (37%)
	64 ps (25%)	>>3 ns (3%)	>>3 ns (7%)
PTB7:PCBM	<<160 fs (89%)	40 ps (23%)	40 ps (12%)
	1.7 ps (11%)	1730 ps (52%)	1730 ps (50%)
		>>3 ns (25%)	>>3 ns (37%)

The first excitation wavelength was at 600 nm (2.07 eV) for the aforementioned TA measurements, which is ≈0.3 eV higher in energy than the absorption onset near the (0,1) vibronic peak. The second excitation wavelength was 695 nm (1.78 eV), which is at the (0,0) vibronic peak. The TA spectra of PTB7:PCBM using 600 nm and 695 nm excitation pumps are shown in Figure 4c,d, respectively. The excitation wavelength dependent EX and CS dynamics in PTB7(cb) was also investigated with the same excitation wavelengths, but no appreciable effects are observed. For PTB7(n), the kinetics trends observed are similar to the solution sample. The kinetics parameters for PTB7(n) and PTB7:PCBM (Table 3) show a slightly increased CR rate in the former, and the main difference for the 695 nm excitation is in the amplitude and time constant of the component with the fastest decay time constant.

The most obvious excitation wavelength dependent dynamic behavior is observed in the cation signal for the CS state in the TA spectrum of PTB7:PCBM. While the EX state dynamics there remains unchanged, dynamics of the CS and CT states show significantly shorter decay time constants under 695 nm light excitation versus 600 nm excitation. Unlike the CS state TA features under 600 nm excitation, with the peak position red-shifted continuously and a rise of the signal with a 116-ps time constant, the CS state TA kinetics under the 695 nm excitation show no detectable rise time, but a modest dynamic red-shift of 0.023 eV (23 nm) from 1.125 eV or 1105 nm to 1.102 eV or 1128 nm, with time constants of 10 ps and 260 ps, respectively. The initial TA peak for the CS state is centered at approximately the same position using both excitation wavelengths; however, the peak position shift with 695 nm light excitation is only ≈1/2 of that with 600 nm excitation. The width of the CS peak increases from 0.136 eV to 0.196 eV under 600 nm excitation while the CS peak increases from 0.112 eV to 0.128 eV under the 695 nm excitation. The peak broadening is significantly larger (65%) using 600 nm excitation versus that at 695 nm excitation.

4. Film Microstructural Studies Using Grazing Incidence X-Ray Scattering

4.1. Experimental GIXS Procedures

Grazing-incidence small-angle X-ray scattering (GISAXS) and wide-angle X-ray scattering (GIWAXS) measurements were performed using beamline 8-ID-E at the Advanced Photon Source (APS) at Argonne National Laboratory.[68] The photon energy is 7.35 keV (λ = 1.6868 Å). Samples were examined under ambient, with a Pilatus 1M detector (Dectris) with pixel size 172 µm × 172 µm used to collect the two-dimensional scattering image. For GISAXS, the sample-dectector distance is 2185 mm and the beam size is 100 µm (h) × 50 µm (v), while for GIWAXS the sample-detector distance is 204 mm and the beam size is 200 µm (h) × 20 µm (v). Typically, two images with a vertical offset were used to avoid gaps in the detector, which consists of 10 modules. Flat field, solid angle and detector efficiency corrections were applied to the images, the images were combined and converted to q-space with the GIXSGUI package for MATLAB.[68] Further processing used local IgorPro software. Reflectivity scans were also recorded to determine the optimal incident angle for data collection. The films were illuminated at an incident angle of about 0.2°.

4.2. PTB7 Morphology: Optimization by Small, Low-Density Ordered Domains in Copolymer Systems

The two-dimensional GIXS images from the films can be analyzed according to the relationship between the scattering vector q, and the d spacing, $q = 2\pi/d$. PTB7(n) films show two distinct scattering features (**Figure 9**a): 1) an out-of-plane broad peak centered at q_z = 1.61 Å^{-1} (d = 3.9 Å) due to π–π stacking of the conjugated polymer backbone (the (010) plane), and 2) in-plane arcs centered at q_y = 0.32 Å^{-1}(d = 1.96 nm) due to the spacing between polymer backbones in the horizontal plane defined by the aliphatic pendent substituents of the polymer domains (the (100) plane). The vertical and horizontal linecuts of the GIXS images for PTB7(n) and PTB7:PCBM films are shown in Figure 9c,d, respectively. The q value of the peak which corresponds to aliphatic spacing also varies due to different degrees of the interdigitation of the polymer substituents. We reported previously that the PTB polymer series films show enhanced "π-face-down" orientations, which maximize the charge transfer from the active layer to the OPV electrode.[20] This polymer orientation is evident principally in the out-of-plane feature due to the π–π stacking in the vertical direction. The intensity of this feature is substrate-dependent from preliminary studies suggesting that the π–π stacking is mainly at the interface to the substrate, with the bulk film mostly disordered.[22,51] The intensity of the peak at q_y = 0.32 Å^{-1} (d = 1.96 nm) is maximal near the q_z = 0 plane, indicating that the chains are oriented in the plane of the polymer backbone. The broad distribution of this intensity along this arclike feature shows that the orientational uniformity of the aliphatic chains is very weak for PTB7 due to the branched pendent groups. In comparison, PTB1 in this series contains

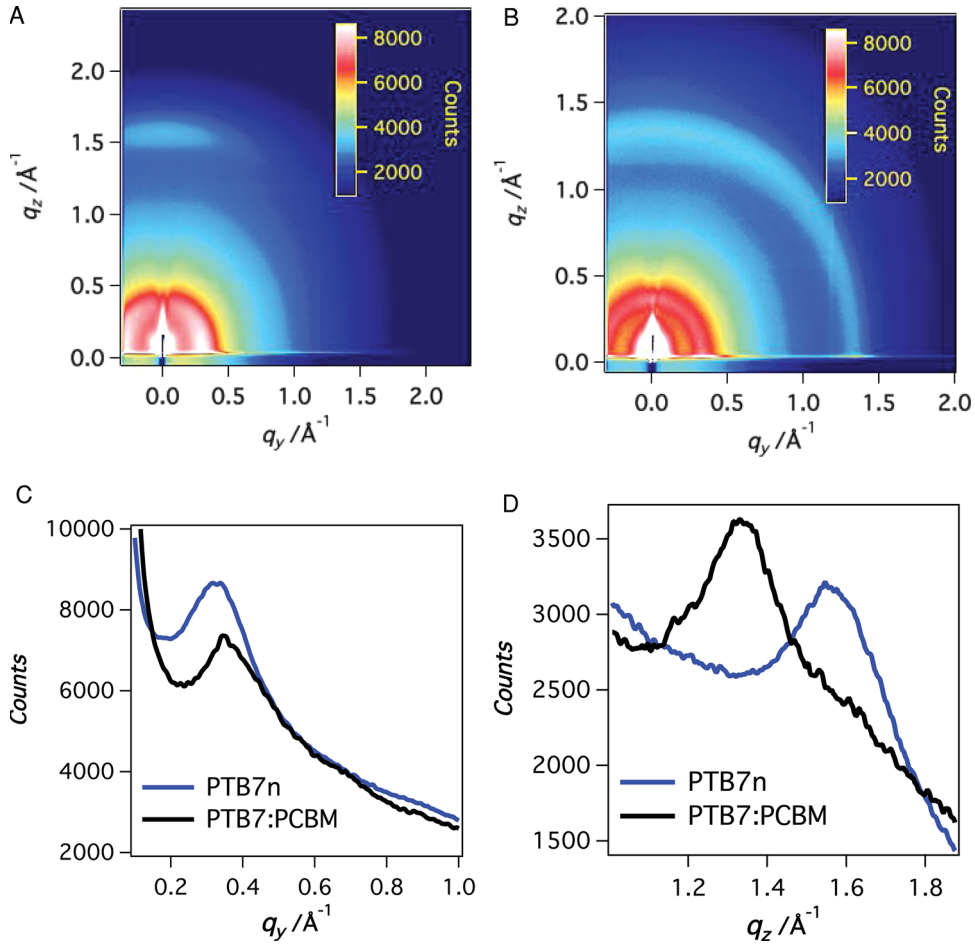

Figure 9. A) GIWAXS results for PTB7(n) and B) PTB7:PCBM. The π-stacking is observed in the z (vertical) direction in the neat films at a scattering vector $q_z = 1.61$ Å^{-1}. The blended BHJ films exhibit a second peak at $q_z = 1.4$ Å^{-1}, due to PCBM. C) Horizontal and D) vertical linecuts of the films.

linear instead of branched pendent groups, and exhibits more order in the aliphatic substituent spacing.[20] Therefore, the branched side chains lower the PTB7 domain crystallinity. Nevertheless, the presence of these peaks shows that very small nanocrystalline domains do exist in the films, mostly oriented parallel to the substrate.

The coherence length of the aliphatic chain spacing (100) has been estimated using Scherrer analysis (Equation 2), where D is the coherence length, λ is the X-ray wavelength, β is the FWHM of the scattering feature in radians (2θ), and θ is the scattering angle.

$$D = \frac{0.9\lambda}{\beta \cos\theta} \quad (2)$$

Since the GIWAXS setup allows resolution of domain sizes up to 11 nm, the experimental peak widths do not require correction. Using this relationship, the coherence length of the π–π stacking peak for the neat polymer is approximately 2.4 nm, while that of the (100) peak is approximately 2.7 nm. It has been established that the coherence length is typically correlated with the degree of lattice order in the structural domains of these materials, which also affects the film morphology.[69] Note that the coherence lengths determined by the Scherrer analysis are only minimum estimates for the grain size in the film. Disorder in the nanocrystalline domainscan also contribute to peak broadening but cannot be determined from a single order of the diffraction.

When PTB7 is blended with PCBM in BHJ films, the most prominent GIXS feature that emerges is a broad isotropic ring centered at $q = 1.4$ Å^{-1} ($d = 4.49$ Å), which is due to the PCBM in the film. The scattering features of the BHJ films are dramatically altered from those in the neat PTB7 films. First, the arc-like feature centered at $q = 0.32$ Å^{-1} ($d = 1.96$ nm) in the neat polymer film due to the spacing between the polymer chains with the pendant aliphatic groups becomes more isotropic in the blended film and centered at a slightly increased q value of 0.37 Å^{-1} (1.70 nm), indicating a greater degree of interdigitation of the aliphatic side chains (Figure 9c). Second, the π–π stacking peak centered at $q = 1.61$ Å^{-1} ($d = 3.90$ Å) in the neat polymer film now overlaps significantly with the isotropic ring due to PCBM (Figure 9d). Although the overall intensity from sample to sample can vary by experimental factors such as critical angle differences and surface roughness,

Adv. Funct. Mater. **2013**,
DOI: 10.1002/adfm.201301820

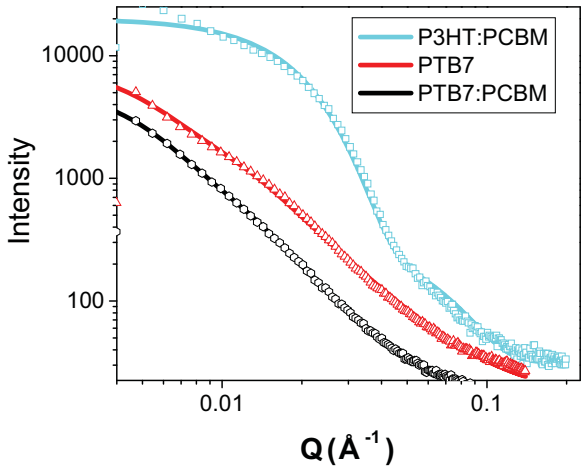

Figure 10. The horizontal GISAXS linecuts for PTB7 films as labeled. For comparison, the same information for P3HT is shown.

the relative decrease in amplitude of the π-stacking peak with respect to the PCBM peak indicates partial disruption of PTB7 nanocrystallites in the blended film. Finally, **Figure 10** shows the small angle GIXS horizontal linecuts of PTB7(n) and PTB7:PCBM, along with the same linecut of a P3HT:PCBM BHJ film for comparison. In the P3HT:PCBM film, the domain dimension is approximately 8 nm as shown by the "Gunier knee" evident in this q region. The small angle GIXS is typically dominated by the PCBM domains,[70–73] so this result determines the domain size of the PCBM in the film. In contrast, the linecuts from PTB7(n) and PTB:PCBM films do not exhibit a Guinier knee feature. Instead, the slope of the curve for both PTB7 films could be fit using a Porod analysis.[74] The slope of the form factors are in the range of 2.1–2.5 nm, which indicates the mass fractal nature of the domains in these films. The presence of fractal domains is consistent with the presence of intermingled domains that have a large surface area between the donor–acceptor domains.

5. New Charge Transfer Mechanisms Elucidated in High-Efficiency Copolymer Systems

The above results from the PTB7 investigations in three different media provide a wealth of information regarding the nature of the various transient species involved in charge-generating processes in high-PCE OPV materials. The combined structural and dynamics results reveal the mechanisms for carrier formation and charge separation on time scales of 10^{-13}–10^{-9} s, and uncover the structural influences of polymer packing on the dynamic processes in the films. We focus here on three processes in detail: 1) the nearly instantaneous formation of intra- and intermolecular charge separation in PTB7(n), 2) the stepwise dissociation of the bound h–e pair or polaron pair in the BHJ PTB7:PCBM films due to the reduced exciton binding energy in the "in-chain donor–acceptor" copolymers such as PTB7, 3) the morphological dependence of charge transfer and separation in PTB7 films. What is learned by analyzing these processes will provide new models to optimize copolymers for OPV applications.

5.1. Intramolecular Versus Intermolecular Charge Transfer in PTB7 as a Function of Medium

Based on the results discussed above, it is evident that PTB7 CS state formation in different media can occur via both intramolecular and intermolecular charge transfer mechanisms. The nearly instantaneous CS state formation observed in both PTB7(cb) and PTB7(n) is principally due to initial intramolecular charge separation arising from ultrafast exciton polarization originating in the BDT donor–TT acceptor electron density gradient along the polymer backbone. Phenomenologically, the polarized exciton can be characterized by an intrinsic dipole moment change in a single repeat unit of the copolymer as described in previous studies.[21,52] In other words, the exciton splitting in all media initially generates a Coulombically bound charge separated h–e pair state with an energy determined by the electrostatic interactions at a certain h–e separation distance, R_{he}. In contrast, the intermolecular CS process observed in the PTB7:PCBM samples is mainly due to the electron transfer from the polymer electron donor to the PCBM electron acceptor as described in the literature.[28,35,75] The roles of CS generation in the different media via the intra- and intermolecular mechanisms are of great importance for understanding OPV functional performance. Exactly how excitons/polarons move and dissociate in BHJ OPV materials with low dielectric constants and amorphous morphologies has been extensively studied.[65,76,77]

One aspect of PTB7:PCBM TA spectroscopy that has not been observed extensively in other polymer systems is the dynamic red-shift of the cation peak in BHJ films. This red-shift suggests a sequential evolution of the CS state involving both intra- and intermolecular mechanisms. When the h–e pairs in the EX state of PTB7 dissociate in the BHJ film, the initial h–e separation distances in an ensemble are likely to have a distribution, because of the diverse polymer and PCBM local structures. On one hand, the driving force from EX enables charge separation, while on the other hand, the electrostatic attractions between holes and electrons promote charge recombination as described by the Onsager model. In order to form free charge carriers, the electrostatic interactions stabilizing the h–e pair must be overcome by other driving forces in this uphill process. As mentioned earlier, the h–e pair dissociation process in the BHJ films is monitored via the time evolution of the energy gap between CS and upper states as evidenced by the spectral red-shift as a function of the delay time. The strength of the electrostatic attraction between the hole in the polymer (cation) and in the electron in the PCBM molecule (anion) can in principle vary due to the local structure and environment, resulting in a variation in the peak position of the TA spectrum cationic peak. The PCBM molecule that accepts the electron from the polymer initially is assumed to be in an immediate close vicinity. Therefore, the polymer CS (cation) signals are observed at early times in the TA spectra. Because the hole is partially bound to the electron on the PCBM moiety, the formation of the "free" or unbound cationic

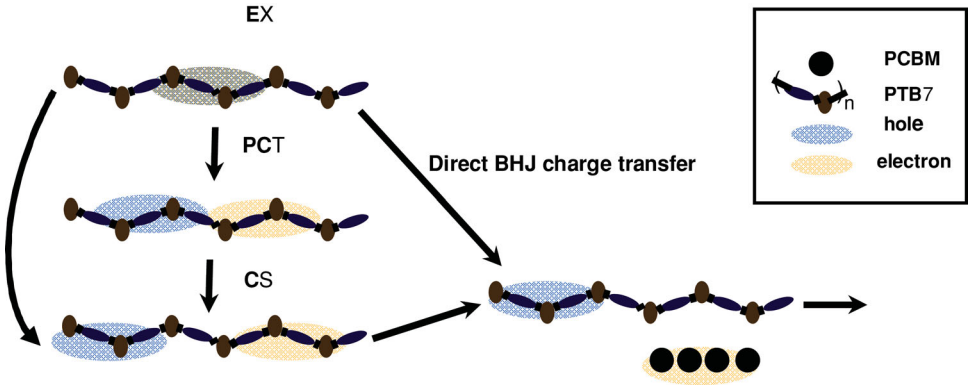

Figure 11. Schematic representation of the exciton, charge transfer, and charge separated states in PTB7:PCBM films. Upon excitation, the excitons almost instantaneously form both intermolecular and intramolecular charge transfer and cationic states. Once the cationic state is formed, the charged species move apart from one another and dissociate. The dissociation process is facilitated by the intramolecular charge transfer and charge separation pathways present in PTB7.

state also corresponds to the formation of the free PCBM anionic state, which, as we have shown, can be measured directly from the spectral shift of the CS state.

In contrast, the kinetics of PTB7(n) CS TA spectra are essentially excitation-wavelength independent, and the dominant intramolecular CS dynamics are not substantially altered by the excitation energy. Therefore, the excitation wavelength dependent CS dynamics in the BHJ films are attributed only to the dissociation of the holes in the polymer cation and the electrons in the PCBM anion. A higher excitation energy provides sufficient excess energy to overcome the Coulombic attractions within the h–e pair and to drive the uphill dissociation to free carriers. Similar effects have been observed in temperature-dependent mobility investigations.[78] The process is reflected in the red-shift in time of the cation spectral feature. At early times, the creation of free carriers can originate from both bound CS and PCT. Lower energy excitation provides little or no excess energy for the h–e pair to escape from Coulombic attractions, so the initially generated CS is less likely to dissociate into charge carriers, but more likely to stay bound and to eventually recombine. Additional CS population in this case will not be generated from PCT, but both CS and PCT decay via the recombination pathway that becomes more prevalent as the rate of free carrier generation is reduced. This result has significant implications on the nature of charge formation and transfer in OPV films.

The relative differences between the peak position in PTB7(cb) and PTB7(n) support the assignment of the cationic state peak. The relative amount of the cationic state in PTB7(cb) is remarkably high. There is a 0.05 eV blue-shift of the cationic state peak in PTB7(n) from 1.07 eV (1160 nm) in PTB7(cb) to 1.12 eV (1110 nm). This blue-shift is a compelling indicator of the bound polaron pair in PTB7(n). The schematic of the CT and CS states in BHJ films are more accurately indicated in the schematic on the bottom of **Figure 11**. The h–e recombination in PTB7(n) is also much faster than in PTB7(cb) and PTB7:PCBM. The addition of the PCBM material separates the electrons and holes energetically, which in turn quenches many of the recombination pathways available in the neat films.

5.2. Reduction of Exciton Binding Energy and Coulombic Interactions in the Polymer Charge Transfer States

Although the nature of charge transfer and separation has been discussed extensively,[38–39,79–89] the stepwise red-shift of the cationic polaron has not been observed in previous reports, to the best or our knowledge. It has been shown that the bound radical pair in P3HT red-shifts on the ns timescale, but the lifetime of this shift has not been described in detail.[35,36,65] In BHJ films, the initial peak position of the cationic state is close to the 1.12 eV (1110 nm) value obtained in PTB7(n), but the final value of 1.09 eV (1145 nm) is close that in PTB7(cb). These findings can be explained by the initial formation of bound charges in PTB7(n), where the neighboring PTB7 polymer strands are close, thus enhancing intermolecular charge separation as well as charge recombination. In contrast, the cation formed upon the photoexcitation of PTB7 in solution will have a much lower probability of undergoing charge recombination via intermolecular processes, primarily due to a large average distance between the cationic and anionic polarons in isolated single polymer strands. When PTB7 is blended with PCBM in the BHJ films, the electron transfer driving force can be approximately described by the Marcus theory,[47,90] as the free energy difference between the EX state and the CT/CS state, plus the reorganization energy between the two states, enables intermolecular charge separation processes that compete favorably with intra- and intermolecule charge recombination. Therefore, recombination is minimized by the structural reorganization energy barrier from the CS state to the ground state. Because of the driving force for the charge separation in the presence of PCBM, the initially generated intramolecular bound polarons can undergo further charge separation/dissociation, resulting in a CS state with its energy inversely proportional to the h–e separation distance. Therefore, the red-shift on the timescale of ≈100 ps is attributable to the dissociation of the bound polarons which are stabilized by Coulombic attractive forces into free polarons. The anionic polarons were not observed in the wavelength range of the present experiments, but were observed in previous studies of other conjugated polymers. For example, some anionic polarons in higher bandgap materials exhibit

DOI: 10.1002/adfm.201301820

characteristic TA features in the 1600 nm region.[91] Based on these studies, we estimate that the TA features of the anionic state in PTB7 could appear at in even lower energy regions, for example, >1700 nm, which is outside the accessible wavelength region of these experiments. However, the dynamics obtained by monitoring the cationic state give sufficient evidence of the energetic shift and carrier separation in these films.

The dissociation of polarons is typically described by the Onsager-Braun relationship,

$$k_d(E) = k_r \frac{3}{4\pi a^3} e^{-\frac{E_B}{k_B T}} \left[1 + b + \frac{b^2}{3} + \frac{b^3}{18} + \cdots\right] \quad (3)$$

where k_d is the polaron dissociation rate constant, E is the local internal electric field, a is the initial h–e separation distance in the bound polaron after the exciton splitting, E_B is the binding energy for the h–e pair, $b = e^3E/8\,\pi\,\langle\varepsilon\rangle\,\varepsilon_0\,k_B{}^2T^2$, ($k_B$ is the Boltzmann constant, T is the temperature) and the bracket contains the first-order Bessel function as an approximation, k_r is the polaron recombination rate constant, and e the elementary charge. E is estimated to be 4×10^6 V cm^{-1}, obtained by dividing the open circuit voltage, V_{oc}, by the film thickness in the PTB7 OPV. Because $1/k_r$ is >3 ns beyond the probe delay time range in our experiments, its value cannot be accurately measured. Instead, k_r is estimated using the relationship $k_r = e\,\langle\mu_e + \mu_h\rangle/\varepsilon_o\langle\varepsilon\rangle$, where $\langle\varepsilon\rangle$ is the ensemble averaged dielectric constant of the film and ε_o is the vacuum permitivity constant, μ_e and μ_h are the electron and hole mobilities of the film, respectively. The average ground state dipole moment for conducting polymers is typically 3–4 Debyes. μ_h of PCBM is 2×10^{-7} m^2 V^{-1} s^{-1} while μ_e of PTB7 is 5.8×10^{-8} m^2 V^{-1} s^{-1}.[44] $\langle\varepsilon\rangle$ for PCBM is 3.9[92] while that for PTB7 is 4.1.[93] Therefore, $\langle\varepsilon\rangle = 4$ is assumed for the BHJ films, and k_r is estimated to be on the order of $\approx 1.5 \times 10^{-15}$ m^3 s^{-1} for the PTB7 films. The polaron binding energy is typically estimated using the following relationship:[28]

$$E_B = \frac{e^2}{4\pi\,\langle\varepsilon\rangle\,\varepsilon_0 a} \quad (4)$$

Hence, k_d is dependent on a and E_B. The calculated k_d as a function of a for a film with $\varepsilon = 4$ is shown in **Figure 12**.

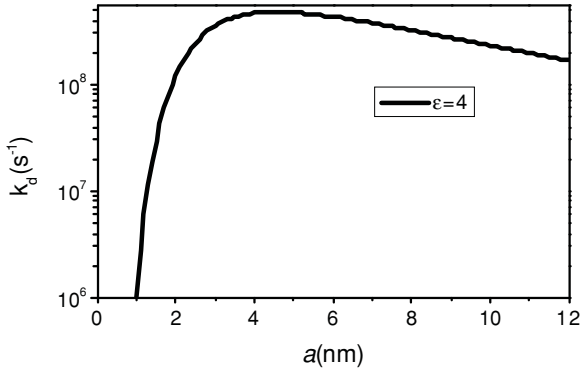

Figure 12. The calculated dissociation rate as a function of the electron-hole radius. The dissociation rates obtained indicate that the electron-hole distance is 4–6 nm in these films.

Although calculated k_d values are known to be lower than the corresponding experimental values,[61] the results reveal k_d trends with h^+–e^- separation distance a for these polarons. For $a < 2$ nm, k_d is very small, indicating a low dissociation probability in the films, while for $a = 2$–6 nm, k_d rises sharply. Finally, when $a > 6$ nm, k_d gradually falls with a. The faster dissociation rate in PTB7 is attributed to the larger initial h^+–e^- separation in the EX state compared to that in homopolymers due to the charge transfer characters between adjacent donor–acceptor blocks in each repeat unit. This stabilizes the intramolecular charge transfer state with pre-separated h^+–e^- character before electron transfer to PCBM. Therefore, electron transfer to PCBM can occur at a longer distance from the hole, because the polaron binding energy is significantly reduced according to the Onsager-Braun model.[61] At excitation energies greater than the driving force for the exciton splitting (e.g., 600 nm excitation), the excess energy can be converted to thermal energy that helps dissociate higher energy polarons. The energy rise of the cationic polaron is 34 meV. At 695 nm excitation, less thermal energy is available for the cationic polaron. The change in the cationic polaron energy is only 19 meV, indicating that the h^+–e^- pair is still partially bound at longer times.

5.3. Morphology Dependence of Charge Transfer and Separation in PTB7

Conventional wisdom regarding optimal BHJ film morphology emphasizes the requirement that the domain sizes be smaller than the exciton diffusion length to enable excitons to reach to the donor:acceptor boundaries, for splitting into holes and electrons.[94] In contrast, when the domain sizes become too small, the pathways for hole and electron transport may be too fragmented and hindered for efficient transport. Many studies have focused on finding the optimum balance between domain size and charge carrier mobility, as in numerous studies of P3HT morphology control.[95–97]While the interplay between BHJ domain size and crystallinity has attracted much attention,[22,71,98–115] many key issues have not been fully resolved. The optimal morphology for P3HT or similar materials in the OPVs was achieved using highly regioregular polymers to control the π–π stacking direction and crystallinity, both of which are influenced by the degree of P3HT regioregularity[116] and PCBM intercalation.[102] It has been shown that the optimal morphology for the benchmark regioregular P3HT:PCBM is large, highly crystalline domains which are achieved via annealing.

Note however that PTB7 exhibits distinctively different structural characteristics from those of P3HT according to GIXS results. Interestingly, the optimal morphology for PTB7:PCBM device performance is very different from that of the regioregular P3HT:PCBM devices, but similar to that of the regiorandom P3HT polymers which are more amorphous, with domain sizes of ≈2 nm, much smaller than the 10–20 nm domain sizes in high-efficiency P3HT:PCBM films. The high crystallinity required in the highest performing P3HT:PCBM OPVs is not seen or required in the highest performing PTB7:PCBM OPVs. An earlier study on another PTB derivative, PTB1 with an identical backbone to PTB7 but with different

pendent substituents, showed that the increased crystallinity induced in PTB1:PCBM films by thermal annealing lowered the CS population and OPV PCE by a factor of two.[26] Similar results were here obtained for PTB7:PCBM films, which suggests that a low-crystallinity film morphology for PTB7:PCBM blends enhances device performance. The question then is why these in-chain donor–acceptor copolymers favor a less crystalline morphology.

The internal quantum efficiency, $\eta_{IQE}(\lambda)$, can be expressed as the product of efficiencies of four individual OPV processes

$$\eta_{IQE} = \eta_{ED}\,\eta_{CS}\,\eta_{CT}\,\eta_{CC} \quad (5)$$

where η_{ED}, η_{CS}, η_{CT}, and η_{CC} are the efficiencies for exciton diffusion, charge separation, charge transport, and charge collection processes, respectively. This relationship was originally formulated for model OPVs fabricated from semiconductor bilayer films.[117] The efficiency of each process can be determined separately. Thus, $\eta_{IQE}(\lambda)$ for PTB7 exceeds 90% at most wavelengths in the visible spectrum.[44,118] The exciton diffusion efficiency can be calculated by using $\eta_{ED} = k_t/(\tau_{av}^{-1})$, where the exciton quenching rate constant $k_t = \tau_{av}^{-1} - k_F$, (here, τ_{av} is the average lifetime of singlet excitons, and k_F is the average decay rate constant of singlet excitons). Using an upper limit of 290 fs for the exciton lifetime (using the relationship $\tau_{av} = A_1\tau_1 + A_2\tau_2$ from the exciton dissociation kinetics for PTB7:PCBM, see Table 2) and an exciton decay of 21 ps (obtained from the average kinetics of PTB7(n)), the minimum exciton diffusion quantum efficiency is 98.6%. For OPV systems that undergo ultrafast electron transfer, the charge separation efficiency (η_{CS}) is assumed to be ≈1. For an initially bound polarons, the charge transport efficiency $\eta_{CT} = (k_{CS} - k_{CR}/k_{CS})$, where k_{CS} and k_{CR} are the charge separation and charge recombination rate constants, respectively. The charge separation rate constant is determined by the time constant for the red-shift of the cationic state peak position as described above. For high efficiency PTB7:PCBM films, this time constant is ≈90 ps using the 600 nm light excitation, while the charge recombination time constant is over 3 ns. Using these values, the lower limit of η_{CT} observed in the PTB7:PCBM films is 0.96. Therefore, η_{CC} is calculated to be 0.95. This extrapolated η_{CC} is similar to or higher than that obtained for very high-quality P3HT:PCBM films and much higher than that obtained for regiorandom P3HT:PCBM films.[24,119]

As noted above, the PTB7:PCBM film morphology is significantly more amorphous than in optimized P3HT BHJ films, with the film order lying between that of typical regioregular and regiorandom P3HT:PCBM films. While η_{CC} of regioregular P3HT:PCBM devices is 57–74% without annealing, that of regiorandom P3HT:PCBM devices is only 15%. The following question then arises: why do PTB7:PCBM devices have a η_{CC} over 90% when the overall order of the films is relatively low versus P3HT:PCBM? The answer lies in the role of the intramolecular charge separation in PTB7:PCBM OPV performance. The intramolecular charge separation along a single polymer chain, driven by the donor–acceptor electron density gradient effectively produces polarized excitons with displaced positive and negative charges across the exciton. This lowers the exciton binding energy and results in a longer average separation distance after the exciton splitting. Consequently, the h^+–e^- pairs have a higher dissociation probability and escape from the capture radius, r_c, defined by the Onsager-Braun model as $r_c = e^2/(4\pi\varepsilon\varepsilon_0 k_B T)$ at which carriers can overcome the Coulomb potential barrier, and further separate across different film domains. The value of r_c in conjugated polymers is ≈3.5 nm assuming a dielectric constant of 4, as in most of organic media. Furthermore, the minimum coherence length along the π-stacking direction in PTB7:PCBM films is 2.1 nm from the GIXS results above. In this case, r_c is greater than the coherence length when charge separation occurs, even within a single polymer strand (to be described in detail below). Therefore, the PTB7:PCBM collection efficiency is much greater than the typical 0.15 values reported for regiorandom P3HT. We attribute this difference to the intramolecular charge transfer within the PTB7 backbone chain. Charges are less likely to become trapped in a domain if the carriers are separated because of a) the smaller binding energy associated with this separation, and b) the possibility of the intramolecular carriers to reside on different domains, which is described below. Therefore, the morphology optimization depends directly on the presence of these intramolecular charge transfer states along the polymer backbone chain.

For the PTB7:$PC_{71}BM$ films, the polymer:fullerene weight ratio for optimal performance is 1:1.5, while this ratio is typically 1:1 or 1:0.6 for optimized P3HT:$PC_{71}BM$ or P3HT:$PC_{61}BM$ films. The relative molar ratio of the polymer repeat units:PCBM can be determined from the molecular weights of the two materials. The molecular weights per repeat unit of P3HT and PTB7 are 166.3 and 729 g mol^{-1}, respectively, while the molecular weights for $PC_{61}BM$ and $PC_{71}BM$ are 911 and 1031 g mol^{-1}, respectively. Therefore, there is approximately one PCBM molecule for every PTB7 repeat unit, and for approximately six P3HT thiophene repeat units in their respective optimized BHJ films. Dimension-wise, the lengths of the polymer segments for each PCBM molecule in PTB7 and P3HT are 2 and 2.4 (0.4 × 6) nm, respectively. The average molecular weight of the PTB7 polymer in this study is 97.5 kDa, or 133 repeat units, and the molecular weight of P3HT for high efficiency solar cells is typically 20–90 kDa, or 123–541 repeat units. Thus, the full length of an average PTB7 strand is ≈140 nm while that of a P3HT strand is 50–216 nm, meaning that P3HT can form markedly larger crystalline film domains, each from a single P3HT strand. Considering that the π–π stacking distance for both polymers is less than 0.4 nm, a 10 nm spherical domain can easily accommodate an entire 200 nm P3HT strand if the polymer folds every 23 units. This composite size is well within the bounds of phase-separated states observed in P3HT:PCBM composite films. Using a Scherrer analysis for the GIXS data, we obtain coherence lengths in P3HT as large as 30 π-stacked polymer backbones. In contrast, the composite domain size of the PTB7 is determined to be less than 3 nm, equivalent to 1–2 repeating units, and the coherent π-stacked domain size is 6–8 polymer backbones. Note however that it is impossible to form such small domains from a single PTB7 chain, so that these small domains must be interconnected by amorphous PTB7 strands.

Based on the above discussion, a schematic morphological model is proposed for the BHJ P3HT and PTB series polymers (**Figure 13**). For PTB7, the charge transfer character in each repeating unit facilitates more efficient intramolecular charge separation, mostly along the polymer backbone before electron

DOI: 10.1002/adfm.201301820

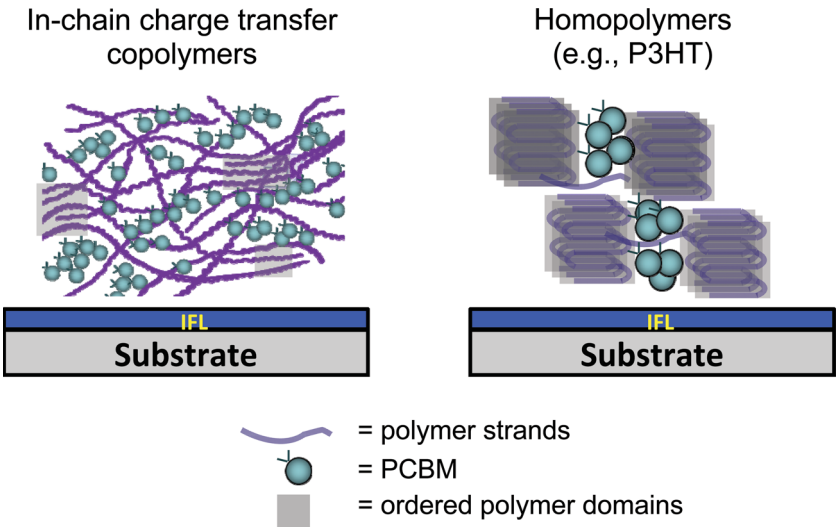

Figure 13. The proposed mechanism of the morphology dependence of a) PTB7 and b) regioregular P3HT. The PTB7:PCBM films have very small domain sizes. The intramolecular charge transfer process can transcend over to different domains, which in turn facilitates charge separation and dissociation.

transfer to the PCBM acceptor. In contrast, the intramolecular charge separation is very inefficient in P3HT or other homopolymers. The conjoined small PTB7 polymer domains facilitate charge separation state formation within a single polymer strand connecting multiple separate crystalline domains in the overall amorphous films. This morphology combined with significant intramolecular charge separation enables a greater average h–e separation distance as the excitons split, with a higher probability for h–e pairs to overcome their Coulombic attraction, and subsequently, the rapid charge separation observed for the PTB7:PCBM films. The intercalation of PCBM among the PTB7 strands is relatively high in this material according to the structural measurements, which can explain why more PCBM is needed to effectively create an efficient acceptor network for optimal charge transport in these films. In comparison, large and highly crystalline polymer domains, such as observed in regioregular P3HT:PCBM, have distinct phase separation with PCBM. In such BHJ films, the less efficient OPV function is typically counterbalanced by the high carrier mobility within the crystalline domains. The relatively small thiophene monomers and relatively flexible connections between them enable each individual polymer strand to fold within the film crystallite. In this motif, carriers could in principle be trapped if no adjacent crystallite is available for them to hop to. The charges are therefore highly localized, so diffusion is expected to be minimal for these materials. Therefore, the OPV performance of P3HT:PCBM active layers benefits from annealing that produces larger, more ordered domains as well as better connected transport channels for holes and electrons. Furthermore, this picture provides the following rationales for device performance optimization with more amorphous PTB7:PCBM films: 1) the repeat unit charge transfer character facilitates the charge separation of the polaronic states, and two polarons can be formed almost instantaneously in different film regions or domains; 2) the morphology of single polymer strands connecting multiple small separate crystalline domains in the overall amorphous films enables PCBM intercalation either by exposure to the acceptor or possibly via polymer templating that helps to organize the PCBM domains. While these domains are quite small, the relatively high PCBM content assures a continuous PCBM network for efficient charge collection in these materials.

6. Conclusions and Outlook

A comprehensive study of exciton splitting and charge transfer dynamics of PTB7, the high-performance BHJ OPV conjugated in-chain donor–acceptor polymer, in different media has been carried out, and the results are correlated with the microscopic polymer packing structure and film morphology. These results imply new kinetic and morphology optimization strategies for charge transfer copolymer OPVs. The interplay between the intra- and intermolecular charge transfer states has significant implications for how to optimize BHJ morphology, with the higher degree of intramolecular charge separation within copolymer materials such as PTB7 lowering the constraints on exciton diffusion in BHJ devices. Therefore, the interfacial area of the donor–acceptor domains becomes a major component that limits organic solar cell efficiency.

Acknowledgements

This research is supported by the ANSER Center, an Energy Frontier Research Center funded by the U.S. Department of Energy, Office of Science, Office of Basic Energy Sciences, under Award Number DE-SC0001059. A part of laser and laboratory equipment is supported by the Division of Chemical Sciences, Office of Basic Energy Sciences, the U.S. Department of Energy under contract DE-AC02–06CH11357 (for L.X.C.). The gift from Intel Corporation to L.X.C. and L.Y. is greatly appreciated to enable a part of materials synthesis and film fabrication. The authors thank Dr. D. J. Gosztola for his help in the Center for Nanoscale Materials at Argonne National Laboratory. The use of the facilities at the Center for Nanoscale Materials and the Advanced Photon Source of Argonne National Laboratory was supported by the U.S. Department of Energy, Office of Science, Office of Basic Energy Sciences, under Contract No. DE-AC02–06CH11357.

Received: May 28, 2013
Published online:

[1] A. O. Patil, A. J. Heeger, F. Wudl, *Chem. Rev.* **1988**, *88*, 183.
[2] M. Reyes-Reyes, K. Kim, D. L. Carroll, *Appl. Phys. Lett.* **2005**, *87*, 083506.
[3] N. S. Sariciftci, L. Smilowitz, A. J. Heeger, F. Wudl, *Science* **1992**, *258*, 1474.
[4] N. S. Sariciftci, L. Smilowitz, A. J. Heeger, F. Wudl, *Synth. Met.* **1993**, *59*, 333.

[5] G. Dennler, M. C. Scharber, C. J. Brabec, *Adv. Mater.* **2009**, *21*, 1323.
[6] M. C. Scharber, D. Wuhlbacher, M. Koppe, P. Denk, C. Waldauf, A. J. Heeger, C. L. Brabec, *Adv. Mater.* **2006**, *18*, 789.
[7] W. Yin, M. Dadmun, *ACS Nano* **2011**, *5*, 4756.
[8] J. S. Kim, Y. Lee, J. H. Lee, J. H. Park, J. K. Kim, K. Cho, *Adv. Mater.* **2010**, *22*, 540.
[9] S. H. Park, A. Roy, S. Beaupre, S. Cho, N. Coates, J. S. Moon, D. Moses, M. Leclerc, K. Lee, A. J. Heeger, *Nat. Photonics* **2009**, *3*, 1355.
[10] M. Reyes-Reyes, K. Kim, J. Dewald, R. Lopez-Sandoval, A. Avadhanula, S. Curran, D. L. Carroll, *Org. Lett.* **2005**, *7*, 5479.
[11] G. Zhao, Y. He, Y. Li, *Adv. Mater.* **2010**, *22*, 4355.
[12] Y. Liang, Z. Xu, J. Xia, S.-T. Tsai, Y. Wu, G. Li, C. Ray, L. Yu, *Adv. Mater.* **2010**, *22*, E135.
[13] Y. Liang, L. Yu, *Acc. Chem. Res.* **2010**, *43*, 1227.
[14] J. Peet, J. Y. Kim, N. E. Coates, W. L. Ma, D. Moses, A. J. Heeger, G. C. Bazan, *Nat. Mater.* **2007**, *6*, 497.
[15] C. V. Hoven, X. D. Dang, R. C. Coffin, J. Peet, T. Q. Nguyen, G. C. Bazan, *Adv. Mater.* **2010**, *22*, E63.
[16] E. Bundgaard, F. Krebs, *Sol. Energy Mater. Sol. Cells* **2007**, *91*, 954.
[17] Y. Zhu, R. D. Champion, S. A. Jenekhe, *Macromolecules* **2006**, *39*, 8712.
[18] H.-Y. Chen, J. Hou, S. Zhang, Y. Liang, G. Yang, Y. Yang, L. Yu, Y. Wu, G. Li, *Nat. Photonics* **2009**, *3*, 649.
[19] Y. Liang, Y. Wu, D. Feng, S. T. Tsai, H. J. Son, G. Li, L. Yu, *J. Am. Chem. Soc.* **2009**, *131*, 56.
[20] J. M. Szarko, J. Guo, Y. Liang, B. Lee, B. S. Rolczynski, J. Strzalka, T. Xu, S. Loser, T. J. Marks, L. Yu, L. X. Chen, *Adv. Mater.* **2010**, *22*, 5648.
[21] B. S. Rolczynski, J. M. Szarko, H. J. Son, Y. Liang, L. Yu, L. X. Chen, *J. Am. Chem. Soc.* **2012**, *134*, 4142.
[22] M. R. Hammond, R. J. Kline, A. A. Herzing, L. J. Richter, D. S. Germack, H.-W. Ro, C. L. Soles, D. A. Fischer, T. Xu, L. Yu, M. F. Toney, D. M. DeLongchamp, *ACS Nano* **2011**, *5*, 8248.
[23] W. Chen, T. Xu, F. He, W. Wang, C. Wang, J. Strzalka, Y. Liu, J. Wen, D. J. Miller, J. Chen, K. Hong, L. Yu, S. B. Darling, *Nano Lett.* **2011**, *11*, 3707.
[24] J. Guo, H. Ohkita, S. Yokoya, H. Benten, S. Ito, *J. Am. Chem. Soc.* **2010**, *132*, 9631.
[25] J. M. Szarko, J. Guo, B. S. Rolczynski, L. X. Chen, *J. Mater. Chem.* **2011**, *21*, 7849.
[26] J. Guo, Y. Liang, J. Szarko, B. Lee, H. J. Son, B. S. Rolczynski, L. Yu, L. X. Chen, *J. Phys. Chem. B* **2010**, *114*, 742.
[27] S. J. Lou, J. M. Szarko, T. Xu, L. Yu, T. J. Marks, L. X. Chen, *J. Am. Chem. Soc.* **2011**, *133*, 20661.
[28] T. M. Clarke, J. R. Durrant, *Chem. Rev.* **2010**, *110*, 6376.
[29] N. Banerji, S. Cowan, M. Leclerc, E. Vauthey, A. J. Heeger, *J. Am. Chem. Soc.* **2010**, *132*, 17459.
[30] N. Banerji, S. Cowan, E. Vauthey, A. J. Heeger, *J. Phys. Chem. C* **2011**, *115*, 9726.
[31] N. Banerji, E. Gagnon, P.-Y. Morgantin, S. Valouch, A. R. Mohebbi, J.-H. Seo, M. Leclerc, A. J. Heeger, *J. Phys. Chem. C* **2012**, *116*, 11456.
[32] O. Mohammed, N. Banerji, B. Lang, E. Nibbering, E. Vauthey, *J. Phys. Chem. A* **2006**, *110*, 13676.
[33] A. A. Paraecattil, S. Beaupré, M. Leclerc, J.-E. Moser, N. Banerji, *J. Phys. Chem. Lett.* **2012**, 2952.
[34] X. Ai, M. C. Beard, K. P. Knutsen, S. E. Shaheen, G. Rumbles, R. J. Ellingson, *J. Phys. Chem. B* **2006**, *110*, 25462.
[35] H. Ohkita, S. Cook, Y. Astuti, W. Duffy, S. Tierney, W. Zhang, M. Heeney, I. McCulloch, J. Nelson, D. D. C. Bradley, J. R. Durrant, *J. Am. Chem. Soc.* **2008**, *130*, 3030.
[36] H. Ohkita, J. Kosaka, J. Guo, H. Benten, S. Ito, *J. Photonics Energy* **2011**, *1*, 011118.
[37] D. Veldman, O. Ipek, S. C. J. Meskers, J. Sweelssen, M. M. Koetse, S. C. Veenstra, J. M. Kroon, S. S. van Bavel, J. Loos, R. A. J. Janssen, *J. Am. Chem. Soc.* **2008**, *130*, 7721.
[38] J. M. Winfield, A. Van Vooren, M. J. Park, D. H. Hwang, J. Cornil, J. S. Kim, R. H. Friend, *J. Chem. Phys.* **2009**, *131*, 035104.
[39] X. Y. Zhu, Q. Yang, M. Muntwiler, *Acc. Chem. Res.* **2009**, *42*, 1779.
[40] J. M. Hodgkiss, G. L. Tu, S. Albert-Seifried, W. T. S. Huck, R. H. Friend, *J. Am. Chem. Soc.* **2009**, *131*, 8913.
[41] D. C. Coffey, A. J. Ferguson, N. Kopidakis, G. Rumbles, *ACS Nano* **2010**, *4*, 5437.
[42] W. J. Mitchell, A. J. Ferguson, M. E. Kose, B. L. Rupert, D. S. Ginley, G. Rumbles, S. E. Shaheen, N. Kopidakis, *Chem. Mater.* **2009**, *21*, 287.
[43] Y. Liang, D. Feng, Y. Wu, S.-T. Tsai, G. Li, C. Ray, L. Yu, *J. Am. Chem. Soc.* **2009**, *131*, 7792.
[44] Y. Liang, Z. Xu, J. Xia, S. T. Tsai, Y. Wu, G. Li, C. Ray, L. Yu, *Adv. Mater.* **2010**, *22*, E135.
[45] D. Birnbaum, B. E. Kohler, *J. Chem. Phys.* **1992**, *96*, 2492.
[46] M. Scharber, D. Wuhlbacher, M. Koppe, P. Denk, C. Waldauf, A. Heeger, C. Brabec, *Adv. Mater.* **2006**, *18*, 789.
[47] C. Risko, M. D. McGehee, J.-L. Bredas, *Chem. Sci.* **2011**, *2*, 1200.
[48] J. D. Servaites, M. A. Ratner, T. J. Marks, *Appl. Phys. Lett.* **2009**, *95*, 163302.
[49] J. D. Servaites, M. A. Ratner, T. J. Marks, *Energy Environ. Sci.* **2011**, *4*, 4410.
[50] M. A. Green, K. Emery, Y. Hishikawa, W. Warta, E. D. Dunlop, *Prog. Photovoltaics* **2012**, *20*, 606.
[51] C. Piliego, T. W. Holcombe, J. D. Douglas, C. H. Woo, P. M. Beaujuge, J. M. J. Frechet, *J. Am. Chem. Soc.* **2010**, *132*, 7595.
[52] B. Carsten, J. M. Szarko, H. J. Son, W. Wang, L. Lu, F. He, B. S. Rolczynski, S. J. Lou, L. X. Chen, L. Yu, *J. Am. Chem. Soc.* **2011**, *133*, 20468.
[53] R. F. Service, *Science* **2011**, *332*, 293.
[54] B. Carsten, J. M. Szarko, L. Lu, H. J. Son, F. He, Y. Y. Botros, L. X. Chen, L. Yu, *Macromolecules* **2012**, *45*, 6390.
[55] There were no noticeale differences of these samples with encapsulated samples that were never exposed to air in the kinetic or spectral data under the time and energy range we used to perform these experiments.
[56] L. Rothberg, in *Primary Photoexcitations in Conjugated Polymers: Molecular Exciton versus Semiconductor Band Mode*, (Ed: N. S. Sariciftci), World Scientific, Singapure **1998**, p 129.
[57] M. J. Bedard-Hearn, F. Sterpone, P. J. Rossky, *J. Phys. Chem. A* **2010**, *114*, 7661.
[58] F. Sterpone, M. J. Bedard-Hearn, P. J. Rossky, *J. Phys. Chem. A* **2009**, *113*, 3427.
[59] Y. W. Soon, H. Cho, J. Low, H. Bronstein, I. McCulloch, J. R. Durrant, *Chem. Commun.* **2013**, *49*, 1291.
[60] P. F. Barbara, T. J. Meyer, M. A. Ratner, *J. Phys. Chem.* **1996**, *100*, 13148.
[61] C. Deibel, T. Strobel, V. Dyakonov, *Phys. Rev. Lett.* **2009**, *103*, 1.
[62] A. E. Jailaubekov, A. P. Willard, J. R. Tritsch, W.-L. Chan, N. Sai, R. Gearba, L. G. Kaake, K. J. Williams, K. Leung, P. J. Rossky, X. Y. Zhu, *Nat. Mater.* **2012**, *11*, 1.
[63] G. Grancini, M. Maiuri, D. Fazzi, A. Petrozza, H.-J. Egelhaaf, D. Brida, G. Cerullo, G. Lanzani, *Nat. Mater.* **2013**, *12*, 29.
[64] A. A. Bakulin, D. Martyanov, D. Y. Paraschuk, P. H. M. v. Loosdrecht, M. S. Pshenichnikov, *Chem. Phys. Lett.* **2009**, *482*, 99.
[65] A. A. Bakulin, A. Rao, V. G. Pavelyev, P. H. M. van Loosdrecht, M. S. Pshenichnikov, D. Niedzialek, J. Cornil, D. Beljonne, R. H. Friend, *Science* **2012**, *335*, 1340.
[66] T. Strobel, C. Deibel, V. Dyakonov, *Phys. Rev. Lett.* **2010**, *105*, 266602.
[67] B. S. Rolczynski, J. M. Szarko, B. Lee, J. Strzalka, J. Guo, Y. Liang, L. Yu, L. X. Chen, *J. Mater. Res.* **2011**, *26*, 296.

[68] Z. Jiang, X. F. Li, J. Strzalka, M. Sprung, T. Sun, A. R. Sandy, S. Narayanan, D. R. Lee, J. Wang, *J. Synchrotron Radiat.* **2012**, *19*, 627.
[69] S. V. Rakhmanova, E. M. Conwell, *Appl. Phys. Lett.* **2000**, *76*, 3822.
[70] Y. Liang, D. Feng, J. Guo, J. M. Szarko, C. Ray, L. X. Chen, L. Yu, *Macromolecules* **2009**, *42*, 1091.
[71] A. Salleo, R. J. Kline, D. M. DeLongchamp, M. L. Chabinyc, *Adv. Mater.* **2010**, *22*, 3812.
[72] A. J. Parnell, A. J. Cadby, O. O. Mykhaylyk, A. D. F. Dunbar, P. E. Hopkinson, A. M. Donald, R. A. L. Jones, *Macromolecules* **2011**, *44*, 6503.
[73] M.-Y. Chiu, U. S. Jeng, M.-S. Su, K.-H. Wei, *Macromolecules* **2010**, *43*, 428.
[74] G. Beaucage, *J. Appl. Crystallogr.* **1995**, *28*, 717.
[75] T. M. Clarke, F. C. Jamieson, J. R. Durrant, *J. Phys. Chem. C* **2009**, *113*.
[76] C. Deibel, T. Strobel, V. Dyakonov, *Adv. Mater.* **2010**, *22*, 4097.
[77] M. Hallermann, S. Haneder, E. Da Como, *Appl. Phys. Lett.* **2008**, *93*, 053307.
[78] D. Rauh, C. Deibel, V. Dyakonov, *Adv. Funct. Mater.* **2012**, *22*, 3371.
[79] D. M. Adams, L. Brus, C. E. D. Chidsey, S. Creager, C. Creutz, C. R. Kagan, P. V. Kamat, M. Lieberman, S. Lindsay, R. A. Marcus, R. M. Metzger, M. E. Michel-Beyerle, J. R. Miller, M. D. Newton, D. R. Rolison, O. Sankey, K. S. Schanze, J. Yardley, X. Y. Zhu, *J. Phys. Chem. B* **2003**, *107*, 6648.
[80] M. R. Wasielewski, *Chem. Rev.* **1992**, *92*, 435.
[81] L. N. Wang, F. Willig, V. May, *J. Chem. Phys.* **2006**, *124*, 34110.
[82] S. De, T. Pascher, M. Maiti, K. G. Jespersen, T. Kesti, F. Zhang, O. Inganas, A. Yartsev, V. Sundstrom, *J. Am. Chem. Soc.* **2007**, *129*, 8466.
[83] L. N. Wang, F. Willig, V. May, *J. Chem. Phys.* **2007**, *126*, 134110.
[84] A. Ltaief, A. Bouazizi, J. Davenas, P. Alcouffe, *Thin Solid Films* **2008**, *516*, 1578.
[85] S. S. Zade, M. Bendikov, *Chemistry* **2008**, *14*, 6734.
[86] M. Mingebach, S. Walter, V. Dyakonov, C. Deibel, *Appl. Phys. Lett.* **2012**, *100*, 193302.
[87] J. Behrends, A. Sperlich, A. Schnegg, T. Biskup, C. Teutloff, K. Lips, V. Dyakonov, R. Bittl, *Phys. Rev. B* **2012**, *85*, 125206.
[88] J. M. Winfield, A. Van Vooren, M.-J. Park, D.-H. Hwang, J. Cornil, J.-S. Kim, R. H. Friend, *J. Chem. Phys.* **2009**, *131*, 035104.
[89] B. C. Thompson, J. M. Frechet, *Angew. Chem. Int. Ed.* **2008**, *47*, 58.
[90] D. C. Coffey, B. W. Larson, A. W. Hains, J. B. Whitaker, N. Kopidakis, O. V. Boltalina, S. H. Strauss, G. Rumbles, *J. Phys. Chem. C* **2012**, *116*, 8916.
[91] R. Osterbacka, C. An, X. Jiang, Z. Vardeny, **2000**, *287*, 839.
[92] V. D. Mihailetchi, P. W. M. Blom, J. C. Hummelen, M. T. Rispens, *J. Appl. Phys.* **2003**, *94*, 6849.
[93] H. J. Son, W. Wang, T. Xu, Y. Liang, Y. Wu, G. Li, L. Yu, *J. Am. Chem. Soc.* **2011**, *133*, 1885.
[94] A. Pivrikas, N. S. Sariciftci, G. Juška, R. Österbacka, *Prog. Photovoltaics: Res. Appl.* **2007**, *15*, 677.
[95] M.-Y. Chiu, U. S. Jeng, C.-H. Su, K. S. Liang, K.-H. Wei, *Adv. Mater.* **2008**, *20*, 2573.
[96] C.-W. Chu, H. Yang, W.-J. Hou, J. Huang, G. Li, Y. Yang, *Appl. Phys. Lett.* **2008**, *92*, 103306.
[97] P. E. Hopkinson, P. A. Staniec, A. J. Pearson, A. D. F. Dunbar, T. Wang, A. J. Ryan, R. A. L. Jones, D. G. Lidzey, A. M. Donald, *Macromolecules* **2011**, *44*, 2908.
[98] C. Koerner, C. Elschner, N. C. Miller, R. Fitzner, F. Selzer, E. Reinold, P. Bäuerle, M. F. Toney, M. D. McGehee, K. Leo, M. Riede, *Org. Electron.* **2012**, *13*, 623.
[99] N. D. Treat, M. A. Brady, G. Smith, M. F. Toney, E. J. Kramer, C. J. Hawker, M. L. Chabinyc, *Adv. Energy Mater.* **2011**, *1*, 82.
[100] E. D. Gomez, K. P. Barteau, H. Wang, M. F. Toney, Y. L. Loo, *Chem. Commun.* **2011**, *47*, 436.
[101] D. M. DeLongchamp, R. J. Kline, D. A. Fischer, L. J. Richter, M. F. Toney, *Adv. Mater.* **2011**, *23*, 319.
[102] A. C. Mayer, M. F. Toney, S. R. Scully, J. Rivnay, C. J. Brabec, M. Scharber, M. Koppe, M. Heeney, I. McCulloch, M. D. McGehee, *Adv. Funct. Mater.* **2009**, *19*, 1173.
[103] J. H. Oh, Y.-S. Sun, R. D. Schmidt, M. F. Toney, D. Nordlund, M. Könemann, F. Würthner, Z. Bao, *Chem. Mater.* **2009**, *21*, 5508.
[104] C. H. Woo, B. C. Thompson, B. J. Kim, M. F. Toney, J. M. Frechet, *J. Am. Chem. Soc.* **2008**, *130*, 16324.
[105] R. Joseph Kline, M. D. McGehee, M. F. Toney, *Nat. Mater.* **2006**, *5*, 222.
[106]R. C. Nieuwendaal, C. R. Snyder, R. J. Kline, E. K. Lin, D. L. VanderHart, D. M. DeLongchamp, *Chem. Mater.* **2010**, *22*, 2930.
[107] D. S. Germack, C. K. Chan, B. H. Hamadani, L. J. Richter, D. A. Fischer, D. J. Gundlach, D. M. DeLongchamp, *Appl. Phys. Lett.* **2009**, *94*, 233303.
[108] D. M. DeLongchamp, R. J. Kline, E. K. Lin, D. A. Fischer, L. J. Richter, L. A. Lucas, M. Heeney, I. McCulloch, J. E. Northrup, *Adv. Mater.* **2007**, *19*, 833.
[109] D. M. DeLongchamp, Y. Jung, D. A. Fischer, E. K. Lin, P. Chang, V. Subramanian, A. R. Murphy, J. M. Frechet, *J. Phys. Chem. B* **2006**, *110*, 10645.
[110] N. C. Cates, R. Gysel, J. E. P. Dahl, A. Sellinger, M. D. McGehee, *Chem. Mater.* **2010**, *22*, 3543.
[111] A. Mayer, S. Scully, B. Hardin, M. Rowell, M. McGehee, *Mater. Today* **2007**, *10*, 28.
[112] C. Goh, S. R. Scully, M. D. McGehee, *J. Appl. Phys.* **2007**, *101*, 114503.
[113] I. McCulloch, M. Heeney, C. Bailey, K. Genevicius, I. Macdonald, M. Shkunov, D. Sparrowe, S. Tierney, R. Wagner, W. Zhang, M. L. Chabinyc, R. J. Kline, M. D. McGehee, M. F. Toney, *Nat. Mater.* **2006**, *5*, 328.
[114] C. Goh, R. J. Kline, M. D. McGehee, E. N. Kadnikova, J. M. J. Fréchet, *Appl. Phys. Lett.* **2005**, *86*, 122110.
[115] K. M. Coakley, M. D. McGehee, *Chem. Mater.* **2004**, *16*, 4533.
[116] Y. Kim, S. Cook, S. M. Tuladhar, S. A. Choulis, J. Nelson, J. R. Durrant, D. D. C. Bradley, M. Giles, I. McCulloch, C. S. Ha, M. Ree, *Nat. Mater.* **2006**, *5*, 197.
[117] P. Peumans, A. Yakimov, S. R. Forrest, *J. Appl. Phys.* **2003**, *93*, 3693.
[118] J. D. Servaites, B. M. Savoie, J. B. Brink, T. J. Marks, M. A. Ratner, *Energy Environ. Sci.* **2012**, *5*, 8343.
[119] J. Guo, H. Ohkita, H. Benten, S. Ito, *J. Am. Chem. Soc.* **2010**, *132*, 6154.